A potential biosorbent from *Moringa oleifera* pod husk for crystal violet adsorption: Kinetics, isotherms, thermodynamic and desorption studies

Adisak Keereerak, Watchanida Chinpa*

Department of Materials Science and Technology, Faculty of Science, Prince of Songkla University, Hat Yai, Songkhla 90110 Thailand

*Corresponding author, e-mail: watchanida.c@psu.ac.th

ABSTRACT: *Moringa oleifera* pod husk (MOPH), an agricultural waste, is presented as a biosorbent for the adsorption of crystal violet (CV) in water. MOPH was characterized using Scanning electron microscopy (SEM), Fourier transform infrared spectroscopy (FT-IR) and Brunauer-Emmett-Teller (BET) analysis. The effects of adsorption parameters on adsorption capacity were optimized. Adsorption of CV by MOPH was rapid in the first 10 min, and equilibrium was approached within 60 min at all initial CV concentrations. The adsorption kinetics study revealed a good correlation between the pseudo-second order model and the experimental results. The maximum monolayer capacity obtained by Langmuir model was 156.25 mg/g at 25 °C. The negative values of thermodynamic parameters indicated a spontaneous and exothermic sorption process. The desorption of CV from MOPH was highest in aqueous acetic acid solution, and the re-adsorption study confirmed the reusability of the MOPH biosorbent. Taking into account its abundance, low cost, non-toxicity and its effectiveness and reusability based on the present results, MOPH can be regarded as a promising biosorbent for the CV removal.

KEYWORDS: *Moringa oleifera* pod husk, biosorbent, crystal violet, adsorption

INTRODUCTION

Crystal violet (CV), a cationic dye, is extensively used in textile dyeing, paper printing, veterinary medicine and biological stain [1]. The effluents released from the utilization of CV contain poisonous and non-biodegradable dye and compounds, which adversely affect the environment and the quality of human life. Many routes such as biological processes, membrane separation, coagulation, photo-catalytic degradation, photo-oxidation and adsorption can be used to eliminate dye from wastewater [2]. Adsorption is frequently used because it is inexpensive, easy and effective, and the adsorbents could be derived from various materials [3]. In recent years, lignocellulosic materials from agricultural waste have gained interest as alternative adsorbents since they are inexpensive and abundant. The removal of CV using biomass materials has been frequently published. Adsorption capacities higher than 100 mg/g were not often reported; however, they have been achieved from grapefruit peel [4], wood apple shell (*Feronia acidissima*) [5], coffee waste [6] and almond shell [7].

Moringa oleifera (MO) is a member of the family

Moringacae. The leaves, pods and seeds of MO are useful for medical and nutritional purposes because they contain a variety of essential phytochemicals [8–10]. Moreover, previous works reported the use of pod, seed and bark of MO as biosorbents. Bhatti et al [8] presented the removal of Zn(II) using MO pod biomass. MO bark (MOB) was successfully applied to separate Ni(II) from aqueous solutions [9]. MO seed was used for sorption of yellow dye tartrazine [11]. Tie et al [12] studied the adsorption of congo red using MO seed cake powder, the residual solids from oil extraction.

To our knowledge, a biosorbent from MO pod husk (MOPH), which is the useless part, has not been reported. This work, therefore, presents a study of MOPH as an alternative adsorbent for the removal of hazardous CV dye. The MOPH was characterized by scanning electron microscopy (SEM), Fourier transform infrared (FT-IR) spectroscopy, Brunauer, Emmett and Teller (BET) analysis and the pH at point zeta charge (pH$_{pzc}$). The effects of adsorption parameters on CV adsorption capacity were determined for the following factors: adsorbent dosage, solution pH, adsorption time, ini-

tial concentration of CV solution and temperature. Adsorption kinetics, isotherms and thermodynamics were investigated. The desorptions of CV from MOPH at different desorption agents and concentrations were also studied, as was the reusability of used MOPH.

MATERIALS AND METHODS

Materials

MO pod used to prepare the adsorbent was collected from the local market. CV cationic dye was from Sigma Aldrich. NaOH, HCl and CH_3COOH were from Labscan. All reagents were used without purification.

Adsorbent preparation

The husks of pod were separated from the fresh pods, followed by water washing. After drying, the MOPH (Fig. 1a) was cut into small pieces and then pretreated with water at 50 °C until colorless water was obtained. The pieces of MOPH were then dried at 50 °C for 24 h (Fig. 1b). Subsequently, they were ground and sieved through a 250 µm sieve. The obtained MOPH powder (Fig. 1c) was stored in a desiccator for further study.

Adsorbent characterization

The morphologies of MOPH were studied using scanning electron microscopy (SEM JSM-5800, JOEL). The chemical groups were analyzed by Fourier transform infrared spectroscopy (FT-IR) (Bruker EQUINOX 55). A laser particle size analyzer (COULTER, LS 230) was carried out to find the particle size of MOPH. The surface area, pore volume and average pore size of MOPH were measured from the Brunauer-Emmett-Teller (BET) method.

The pH_{pzc} of MOPH was evaluated using the pH drift method [13]. MOPH of 0.03 g was filled to 50 ml of 0.1 M NaCl solutions at initial pH ($pH_{initial}$) values from 2–10. After shaking the mixtures for 24 h, pH was measured and noted as the final pH (pH_{final}). The pH_{pzc} was the point where the curve of the plot of pH_{final} versus $pH_{initial}$ crossed the line where pH_{final} and $pH_{initial}$ were equal.

Batch adsorption studies

The adsorption studies were conducted in 120 ml sample bottles to study the effects on CV adsorption of adsorbent dose (0.2–1.8 g/l), pH (2–10), initial CV concentration (50–250 mg/l), adsorption time (5–120 min) and temperature (25, 35, 45 °C). The MOPH was added into sample bottles containing 50 ml of CV solution. After shaking the mixture at 60 rpm, the MOPH was isolated, and the remaining dye in solution was then determined by UV-Vis spectrophotometry (UV 1601) at a wavelength of 588 nm. Adsorption testing was repeated three times in each case.

The dye removal (%) and the adsorption capacity (q, mg/g) were respectively calculated from Eqs. (1) and (2):

$$\text{Dye removal}\,(\%) = \frac{C_0 - C_t}{C_0} \times 100 \qquad (1)$$

$$q = \frac{C_0 - C_t}{m} V \qquad (2)$$

where the amounts of CV in dye solution (mg/l) at initial time and time t were defined as C_0 and C_t, respectively, V is the CV solution volume (l) and m is the mass of adsorbent (g).

Batch desorption studies

CV-loaded adsorbent obtained from adsorption experiments was mixed with 50 ml of desorbing agents (0.5, 1.0, 1.5 and 2.0 mol/l of CH_3COOH, NaOH and NaCl solutions). After shaking, the remaining CV in the solution (C_d, mg/l) was determined. The percentage of desorption was evaluated from the equation (3):

$$\text{Desorption}\,(\%) = \frac{C_d}{C_0 - C_t} \times 100 \qquad (3)$$

RESULTS AND DISCUSSION

Adsorbent characterization

The SEM photographs of MOPH in Fig. 1 show surfaces and cross-sections of MOPH before and after pretreatment with water at 50 °C. Raw MOPH (Fig. 1d) presented a rough surface, but after pretreatment the surface was even rougher (Fig. 1e) and pores are visible in the cross-sectional fractures (Fig. 1h). The SEM results suggest that the pretreatment used in this work partially eliminated lignin, hemicellulose and noncellulosic substances. The SEM micrographs in Fig. 1(f,i) are of MOPH adsorbent in powder form. Using a laser particle size analyzer, the particle size of this powder was found to be 28.35 ± 21.77 µm, which corresponds to the range of size and shape presented in Fig. 1f. The rough surface and numerous pores present in pretreated MOPH might facilitate the adsorption of cationic dyes.

In the FTIR spectra of pretreated MOPH (Fig. 2), the transmittance peaks assigned to the
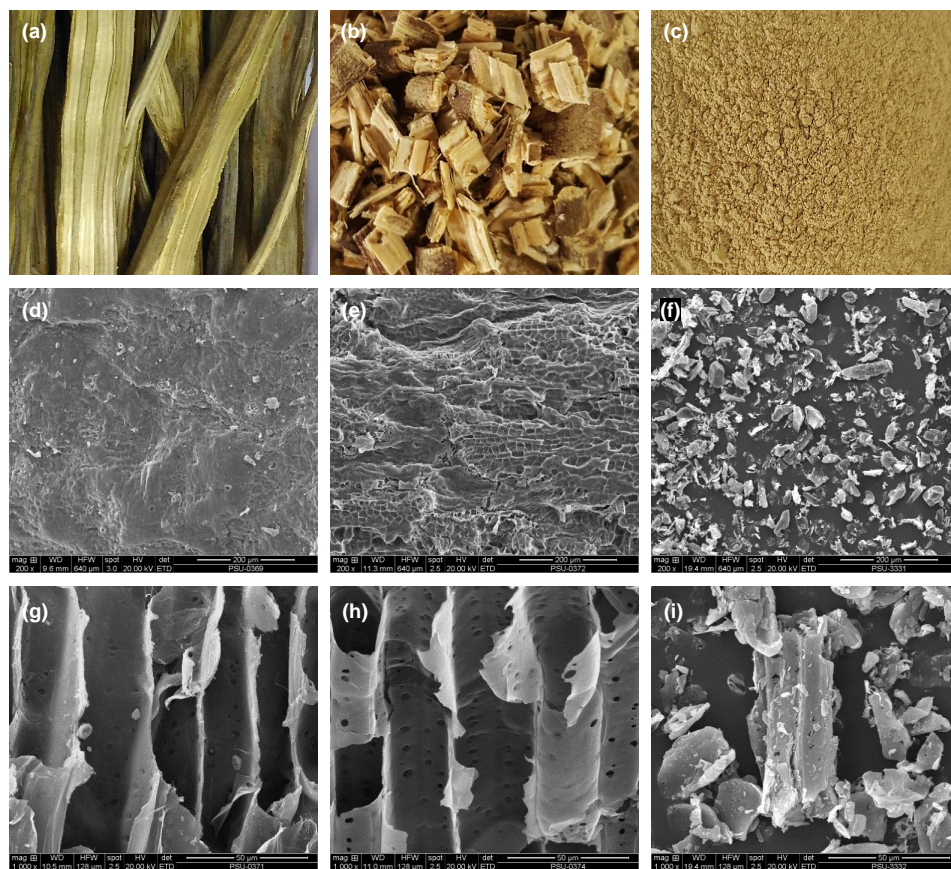
Fig. 1 Photographs and SEM micrographs of surface and cross-section of raw (a,d,g) and pretreated MOPH (b,e,h). Photograph (c) and SEM micrographs at different magnifications (f,i) of pretreated MOPH in powder form.
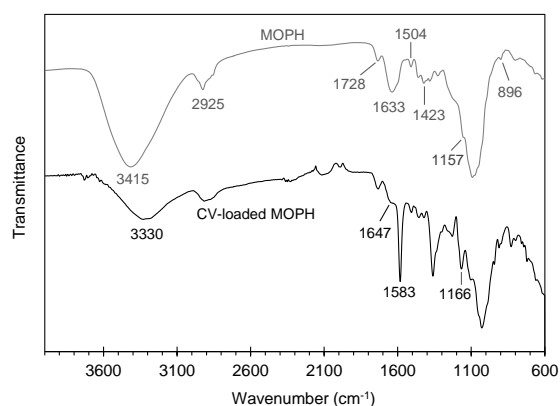
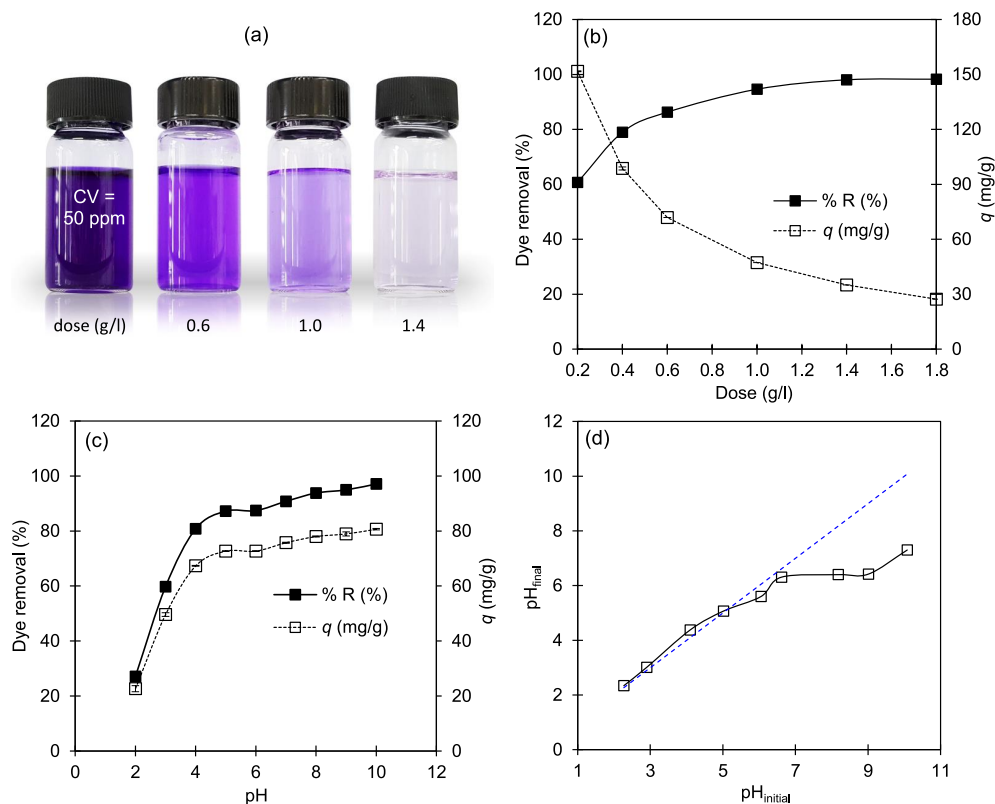**Fig. 2** FTIR spectra of pretreated MOPH powder before and after CV adsorption.

1633 cm^{-1} are attributed to C=O stretching of hemicellulose [14–16]. The peaks around 1504 and 1423 cm^{-1} relate to the C=C aromatic ring of lignin [15, 17], and the band between 1200 and 1059 cm^{-1} indicates C—O stretching in lignocellulose [17]. The peak at 896 cm^{-1} indicates the characteristic structure of cellulose [17]. The hydroxyl and carboxylic groups presented in MOPH could bind with cationic dye via electrostatic interaction and hydrogen boding [6, 18].

The BET surface area and average diameter of pore of MOPH were 2.097 m^2/g and 66.268 Å, respectively. The surface area of MOPH is in the range previously reported for other agricultural wastes, which was 1.38–11.2 m^2/g [18, 19].

Effect of adsorbent dose

Fig. 3a presents the effect of MOPH dose on CV adsorption and demonstrates the high level of CV removal at the higher dosages. The percentage dye

stretching of —OH and C—H groups of lignocellulose are located at about 3415 and 2925 cm^{-1}, respectively [14, 15]. The peaks at 1728 and

Fig. 3 Effect of adsorbent dose (a,b) and pH (c) on CV biosorption; and pH$_{pzc}$ (d) of MOPH.

removal (%R) on a MOPH dosage of 0.2 g/l was 60%. Dye removal increased to 86.27% on a dosage of 0.6 g/l (Fig. 3b). The increase in %R may be attributed to the greater number of available sites for dye-binding and the increased surface area of biosorbent at the higher dosage [20]. At the dosage above 0.6 g/l, %R did not considerably change due to aggregation of adsorbent which would reduce the number of binding sites available to dye molecules. Consequently, increasing the dosage to a certain level reduces the quantity of CV bound onto unit mass of MOPH [18, 20]. From the above results, a MOPH dosage of 0.6 g/l was selected for further studies.

Effect of initial pH

The effect of solution pH on adsorption of CV is shown in Fig. 3c. The pH$_{pzc}$ of MOPH was also determined to elucidate the pH influence on CV uptake, and it was found to be 5.1 (Fig. 3d). We found that both %R and q were low as pH was below pH$_{pzc}$ (Fig. 3c) because the electrostatic repulsion occurred between the positive charges on both MOPH and CV surfaces [18]. When pH of CV solution was greater than 5, the electrostatic inter-

action was promoted between the electronegative biosorbent surface and the cationic dye, resulting in the enhancement of CV adsorption on MOPH [18]. According to the results, a CV solution at pH 6 was used in further studies.

Adsorption kinetics

The kinetic experiment was performed by using a MOPH dose of 0.6 g/l for different time intervals in solutions of different initial CV concentrations (50, 100 and 250 mg/l), all at pH 6 and 25 °C. The result in Fig. 4a demonstrates that adsorption was facilitated by the numerous binding sites on the adsorbent surface during the first 10 min and took place quickly at all initial CV concentrations [4, 20], and the plateau was attained at 60 min assigned as equilibrium time. Fig. 4a shows that increments of initial dye concentration increased dye adsorption capacity. At greater initial amount of CV in the solution, a high driving force existed for dye transfer from the liquid phase to adsorption sites of the adsorbent [20].

The biosorption kinetics of CV on MOPH were studied using pseudo-first order [21] and pseudo-second order [22] kinetic models, which are respec-
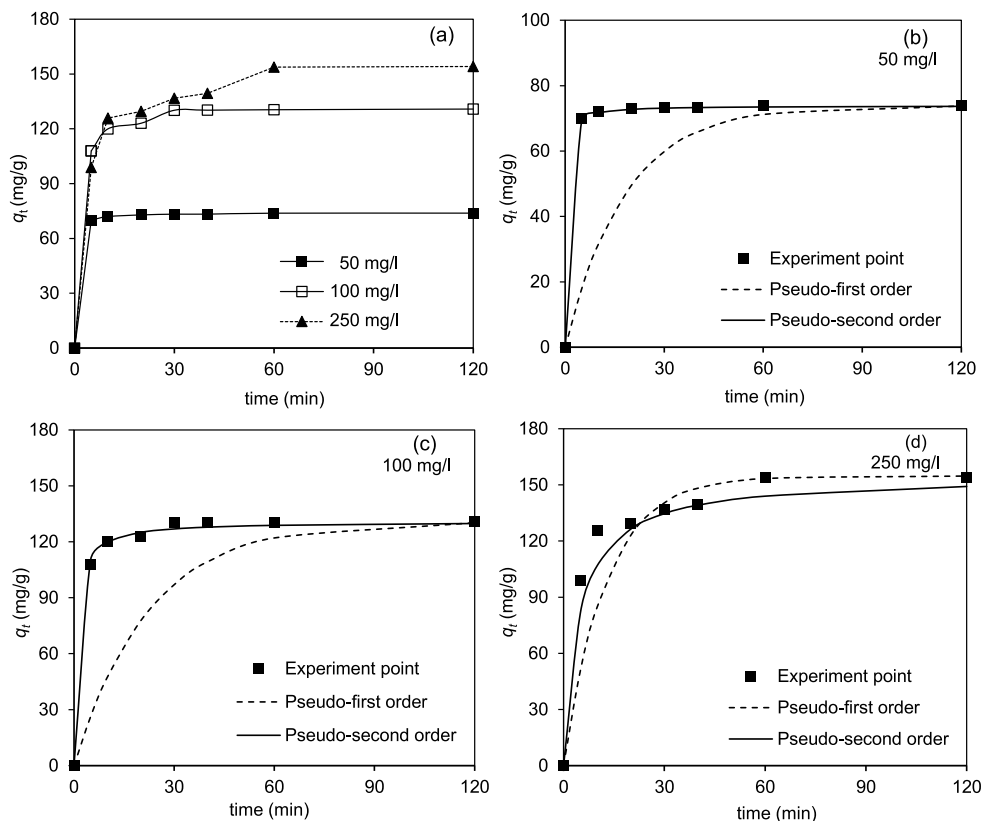
Fig. 4 Effect of contact time at different initial CV concentrations (a) and kinetic curves of CV adsorption on MOPH at 50 mg/l (b), 100 mg/l (c) and 250 mg/l (d).

tively expressed in Eqs. (4) and (5):

$$q_t = q_e \left(1 - e^{-k_1 t}\right) \tag{4}$$

$$q_t = \frac{k_2 q_e^2 t}{1 + q_e k_2 t} \tag{5}$$

in which the mass of CV adsorbed per biosorbent mass (mg/g) were defined as q_e and q_t at equilibrium and at a given time t, respectively. k_1 is the pseudo-first order rate constant (min^{-1}) while k_2 is the rate constant for pseudo-second order (g/mg·min). The experimental kinetic curves and the model kinetic curves are shown in Fig. 4(b–d). Table 1 lists the calculated model constants with the correlation coefficient values (R^2). These findings indicate that the data of the kinetics of adsorption of CV on MOPH is suitably fitted with the pseudo-second order model for all studied initial concentrations ($R^2 \geqslant 0.998$). These results imply that the biosorption process of CV onto MOPH was governed by chemisorption [4].

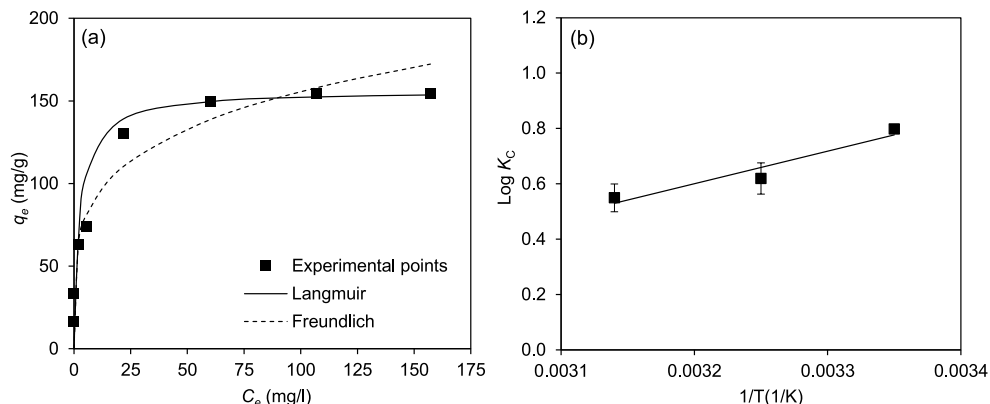**Adsorption isotherms**

Langmuir and Freundlich isotherms [23, 24] were used to study the equilibrium adsorption behavior of CV on MOPH. Adsorption isotherms was studied using adsorption data acquired at a contact time of 120 min to ensure that adsorption equilibrium had been completely achieved. These isotherms are described by the following equations:

$$\text{(Langmuir)} \qquad q_e = \frac{q_{\max} K_L C_e}{1 + K_L C_e} \tag{6}$$

$$\text{(Freundlich)} \qquad q_e = K_F C_e^{1/n} \tag{7}$$

in which C_e (mg/l) is the equilibrium dye concentration in liquid phase, $q_{\max}$ (mg/g) is the maximum adsorption capacity, K_L (l/mg) and K_F ((mg/g)/(mg/l)$^{1/n}$) are the constant values of Langmuir equilibrium constant and the Freundlich, respectively, and n is adsorption intensity. The parameters obtained from both adsorption isotherms are listed in Table 1. Based on the results obtained from the modelled adsorption isotherms (Fig. 5a) and the R^2, in Table 1, the finding points for ad-

Fig. 5 Equilibrium curves (a) and Van't Hoff plot (b) for CV adsorption on MOPH.

Table 1 The pseudo-first order and pseudo-second order models and Langmuir and Freundlich isotherm parameters for CV adsorption on MOPH.

Kinetic model		Pseudo-first order			Pseudo-second order		
C_o (mg/l)	$q_{e,\text{exp}}$ (mg/g)	q_e (mg/g)	k_1 (min^{-1})	R^2	q_e (mg/g)	k_2 (g/mg·min)	R^2
50	73.85	3.92	0.055	0.893	74.07	0.045	0.999
100	130.80	10.05	0.045	0.769	131.58	0.008	0.999
250	154.09	124.59	0.079	0.966	158.73	0.001	0.998

Isotherm model		Langmuir			Freundlich		
Parameter		q_{max} (mg/g)	K_L (l/mg)	R^2	K_F (mg/g)/(mg/l)$^{1/n}$	n	R^2
		156.250	0.372	0.999	55.043	4.431	0.931

sorption of CV on MOPH at equilibrium state fit best with the Langmuir model. This correlation suggests monolayer adsorption behavior. The q_{max} from the Langmuir model was 156.25 mg/g, which is larger than the capacity achieved by some biosorbents with and without chemical treatment (Fig. 6). Moreover, the biosorbent in the present study showed a high adsorption capacity by comparison with effective carbon-based adsorbents that required more materials, energy or processing during fabrication (Fig. 6). The adsorption capacities and equilibrium adsorption times (t_{eq}) presented in Fig. 6 imply that MOPH is an alternative, efficient and environmentally friendly biosorbent for adsorption of CV in water.

Adsorption thermodynamics

The adsorption of CV on MOPH was studied at 298, 308 and 318 K. The Gibb's free energy ($\Delta G°$) can be calculated using Eqs. (8) and (9):

$$K_C = \frac{C_{\text{ae}}}{C_e} \tag{8}$$

$$\Delta G° = -RT \ln K_C \tag{9}$$

$$\ln K_C = \frac{\Delta S°}{R} - \frac{\Delta H°}{RT} \tag{10}$$

where K_C is the constant value at equilibrium. T (K) and R (J/K·mol) are temperature and the gas constant, respectively. The enthalpy ($\Delta H°$) and entropy ($\Delta S°$) can be evaluated using Eq. (10). The slope and intercept from the plot in Fig. 5b yielded the $\Delta H°$ and $\Delta S°$ values, respectively.

The values of $\Delta G°$ were −4.557 (298 K), −3.653 (308 K) and −3.346 kJ/mol (318 K), implying the spontaneous process [19]. The increment of $\Delta G°$ with temperature implies that sorption proceeded more easily at lower temperatures [6]. The $\Delta H°$ value was negative (−22.483 kJ/mol), suggesting that the sorption of CV on MOPH was
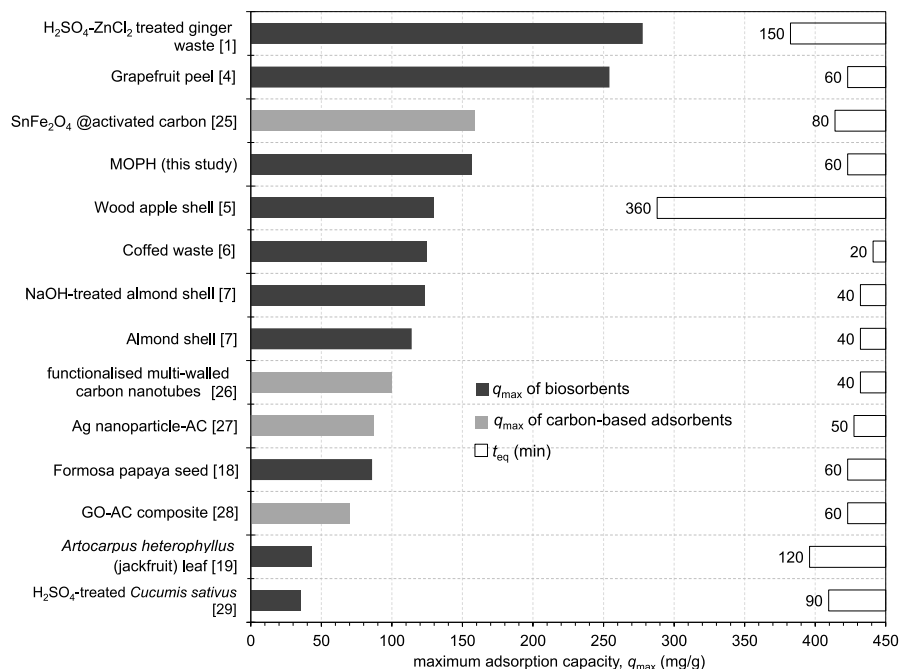
Fig. 6 Maximum adsorption capacity of various adsorbents from Langmuir isotherm model for CV removal and their equilibrium adsorption time.
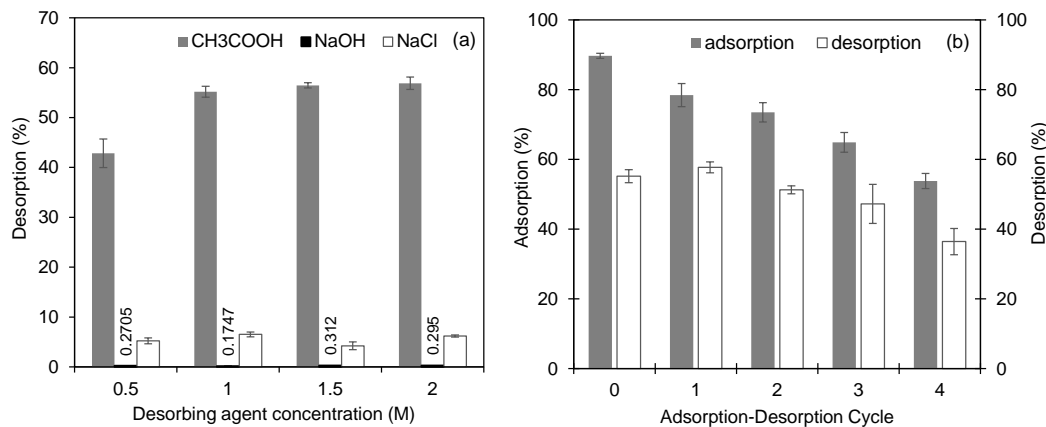
Fig. 7 Effect of desorbing agents and their concentrations on the desorption of CV from MOPH (a) and adsorption-desorption cycle of MOPH by 1 M acetic acid solution (b).

exothermic, and a reduction in randomness of CV at interface between solid and liquid was implied by the negative $\Delta S°$ (-60.446 J/mol·K) [30]. Similar findings were reported for adsorption of CV by coffee waste [6] and *Artocarpus heterophyllus* (jackfruit) leaf powder [19].

Desorption studies

The recovery of adsorbed CV and the regeneration of the MOPH biosorbent were investigated in a

bath desorption study using aqueous solutions of CH_3COOH, NaOH and NaCl at 0.5, 1.0, 1.5 and 2.0 mol/l at 25 °C. The aqueous solution of CH_3COOH exhibited the highest desorption capacity at all concentrations (Fig. 7a). Desorption capacity increased from $42.86 \pm 2.87\%$ for 0.5 mol/l CH_3COOH to $55.17 \pm 1.08\%$ for 1 mol/l CH_3COOH. Thereafter, desorption capacity did not change significantly. The desorption capacity of CH_3COOH solution was attributed to the ability of protons in the acidic
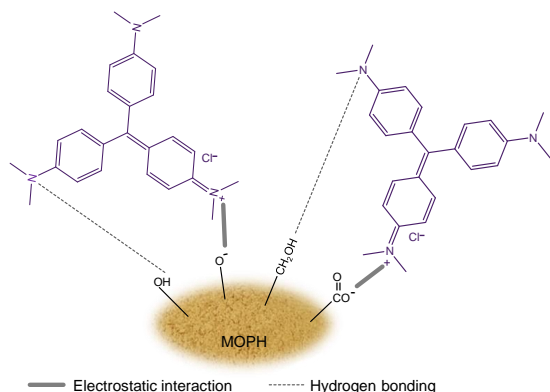
Fig. 8 Proposed adsorption mechanism of CV on MOPH.

solution to replace the cations adsorbed on the adsorbent [31]. The inverse effect was obtained with the NaOH medium. These results suggest the formation of electrostatic attraction between the biosorbent and the cationic dye [18]. Based on the efficient desorption of CV from the biosorbent and low cost, a CH_3COOH solution of 1 M was selected as the desorption agent for further study.

Although CV was not completely desorbed from MOPH, the re-adsorption of MOPH after desorption by 1 M CH_3COOH solution was investigated to evaluate the reusability of the biosorbent. Fig. 7b demonstrates that the adsorption of CV decreased from $89.72 \pm 0.70\%$ in the initial cycle to $78.45 \pm 3.31\%$ in the first recycling. In the fourth cycle, the percentage of dye adsorbed decreased to $53.81 \pm 2.19\%$. Many reasons could describe a reduction of adsorption capacity: occupation by CV molecules of the adsorption sites on the MOPH, degradation of cellulosic biosorbent in acidic media and generation of positive charges on MOPH surface by the acidic desorbing agent [32].

Adsorption mechanism

The adsorption revealed by FTIR in Fig. 2 shows that the peak at 1583 cm^{-1} derived from C—N groups of the CV molecule was observed in CV-loaded MOPH. The peaks present in pretreated MOPH at 3415 and 1633 cm^{-1} moved to 3330 and 1647 cm^{-1}, respectively, in the CV-loaded adsorbent. Moreover, the peak at 1157 cm^{-1} shifted to 1166 cm^{-1}. These results indicated the presence of intermolecular between MOPH and CV. Moreover, the desorption results proved that CV was strongly adsorbed on MOPH. It can be inferred that CV adsorbed on MOPH not only by electrostatic interac-

tion of the positive and negative charges between CV and MOPH but also by hydrogen bonding between nitrogen atoms in CV and hydrogen atoms in hydroxyl or carboxylic groups of MOPH [1, 18]. The proposed adsorption mechanism of CV on MOPH was depicted in Fig. 8.

CONCLUSION

A biosorbent was prepared from *Moringa oleifera* pod husk and investigated for adsorption of CV in water. SEM micrograph of the lignocellulosic biomass revealed a porous and rough surface that facilitated the interaction between CV and MOPH. The MOPH presented a BET surface area of 2.097 m^2/g and pH$_{pzc}$ of 5.1. The adsorption capacity of MOPH increased as pH and initial CV concentration increased. The experimental data agreed well with the pseudo-second order and the Langmuir isotherm models. The thermodynamic study of CV adsorption on MOPH indicated a spontaneous and exothermic process. Desorption of the adsorbed CV and regeneration of the MOPH was possible using acetic acid solution. The results of this study indicated that the environmentally friendly and low cost MOPH biosorbent could provide an alternative means of cationic dye removal.

REFERENCES

1. Kumar R, Ahmad R (2011) Biosorption of hazardous crystal violet dye from aqueous solution onto treated ginger waste (TGW). *Desalination* **265**, 112–118.
2. Oguntimein GB (2015) Biosorption of dye from textile wastewater effluent onto alkali treated dried sunflower seed hull and design of a batch adsorber. *J Environ Chem Eng* **3**, 2647–2661.
3. Bonilla-Petriciolet A, Mendoza-Castillo DI, Reynel-Ávila HE (2017) *Adsorption Processes for Water Treatment and Purification*, Springer, Cham.
4. Saeed A, Sharif M, Iqbal M (2010) Application potential of grapefruit peel as dye sorbent: kinetics, equilibrium and mechanism of crystal violet adsorption. *J Hazard Mater* **179**, 564–572.
5. Jain S, Jayaram RV (2010) Removal of basic dyes from aqueous solution by low-cost adsorbent: wood apple shell (*Feronia acidissima*). *Desalination* **250**, 921–927.

6. Lafi R, ben Fradj A, Hafiane A, Hameed BH (2014) Coffee waste as potential adsorbent for the removal of basic dyes from aqueous solution. *Korean J Chem Eng* **31**, 2198–2206.

7. Ishaq M, Javed F, Amad I, Ullah H, Hadi F, Sultan S (2016) Adsorption of crystal violet dye from aqueous solutions onto low-cost untreated and NaOH treated almond shell. *Iran J Chem Chem Eng* **35**, 97–106.

8. Bhatti HN, Mumtaz B, Hanif MA, Nadeem R (2007) Removal of Zn(II) ions from aqueous solution using *Moringa oleifera* Lam. (horseradish tree) biomass. *Process Biochem* **42**, 547–553.

9. Reddy DHK, Ramana DKV, Seshaiah K, Reddy AVR (2011) Biosorption of Ni(II) from aqueous phase by *Moringa oleifera* bark, a low cost biosorbent. *Desalination* **268**, 150–157.

10. Gopalakrishnan L, Doriya K, Kumar DS (2016) A review on nutritive importance and its medicinal application. *Food Sci Hum Wellness* **5**, 49–56.

11. Reck IM, Paixão RM, Bergamasco R, Vieira MF, Vieira AMS (2018) Removal of tartrazine from aqueous solutions using adsorbents based on activated carbon and *Moringa oleifera* seeds. *J Clean Prod* **171**, 85–97.

12. Tie J, Li P, Xu Z, Zhou Y, Li C, Zhang X (2015) Removal of Congo red from aqueous solution using *Moringa oleifera* seed cake as natural coagulant. *Desalin Water Treat* **54**, 2817–2824.

13. Lopez-Ramon MV, Stoeckli F, Moreno-Castilla C, Carrasco-Marin F (1999) On the characterization of acidic and basic surface sites on carbons by various techniques. *Carbon* **37**, 1215–1221.

14. Khalil HPSA, Ismail H, Rozman HD, Ahmad MN (2001) Effect of acetylation on interfacial shear strength between plant fibres and various matrices. *Eur Polym J* **37**, 1037–1045.

15. Karimi S, Tahir PM, Karimi A, Dufresne A, Abdulkhani A (2014) Kenaf bast cellulosic fibers hierarchy: A comprehensive approach from micro to nano. *Carbohydr Polym* **101**, 878–885.

16. Wang B, Sain M, Oksman K (2007) Study of structural morphology of hemp fiber from the micro to the nanoscale. *Appl Compos Mater* **14**, 89–103.

17. Kaushik A, Singh M (2011) Isolation and characterization of cellulose nanofibrils from wheat straw using steam explosion coupled with high shear homogenization. *Carbohydr Res* **346**, 76–85.

18. Pavan FA, Camacho ES, Lima EC, Dotto GL, Branco VTA, Dias SLP (2014) Formosa papaya seed powder (FPSP): Preparation, characterization and application as an alternative adsorbent for the removal of crystal violet from aqueous phase. *J Environ Chem Eng* **2**, 230–238.

19. Saha PD, Chakraborty S, Chowdhury S (2012) Batch and continuous (fixed-bed column) biosorption of crystal violet by *Artocarpus heterophyllus* (jackfruit) leaf powder. *Colloids Surfaces B Biointerfaces* **92**, 262–270.

20. Saha P, Chowdhury S, Gupta S, Kumar I (2010) Insight into adsorption equilibrium, kinetics and thermodynamics of malachite green onto clayey soil of Indian origin. *Chem Eng J* **165**, 874–882.

21. Lagergren S (1898) Zur theorie der sogenannten adsorption gelöster stoffe. *K Sven Vetenskapsakad Handl* **24**, 1–39.

22. Ho YS, Mckay G (1999) Pseudo-second order model for sorption processes. *Process Biochem* **34**, 451–465.

23. Langmuir I (1918) The adsorption of gases on plane surfaces of glass, mica, and platinum. *J Am Chem Soc* **40**, 1361–1403.

24. Freundlich H, Helle WJ (1939) Adsorption in solution. *J Am Chem Soc* **61**, 2228–2230.

25. Rai P, Gautam RK, Banerjee S, Rawat V, Chattopadhyaya MC (2015) Synthesis and characterization of a novel SnFe$_2$O$_4$@activated carbon magnetic nanocomposite and its effectiveness in the removal of crystal violet from aqueous solution. *J Environ Chem Eng* **3**, 2281–2291.

26. Sabna V, Thampi SG, Chandrakaran S (2016) Adsorption of crystal violet onto functionalised multi-walled carbon nanotubes: equilibrium and kinetic studie. *Ecotoxicol Environ Saf* **134**, 390–397.

27. AbdEl-Salam AH, Ewais HA, Basaleh AS (2017) Silver nanoparticles immobilised on the activated carbon as efficient adsorbent for removal of crystal violet dye from aqueous solutions. A kinetic study. *J Mol Liq* **248**, 833–841.

28. Abd-Elhamid AI, Kamoun EA, El-Shanshory AA, Soliman HMA, Aly HF (2019) Evaluation of graphene oxide-activated carbon as effective composite adsorbent toward the removal of cationic dyes: composite preparation, characterization and adsorption parameters. *J Mol Liq* **279**, 530–539.

29. Smitha T, Santhi T, Prasad AL, Manonmani S (2017) *Cucumis sativus* used as adsorbent for the removal of dyes from aqueous solution. *Arab J Chem* **10**, S244–S251.

30. Chigbundu EC, Adebowale KO (2017) Equilibrium and fractal-like kinetic studies of the sorption of acid and basic dyes onto watermelon shell (*Citrullus vulgaris*). *Cellulose* **24**, 4701–4714.

31. Cechinel MAP, Ulson De Souza SMAG, Ulson De Souza AA (2014) Study of lead (II) adsorption onto activated carbon originating from cow bone. *J Clean Prod* **65**, 342–349.

32. Daneshvar E, Vazirzadeh A, Niazi A, Kousha M, Naushad M, Bhatnagar A (2017) Desorption of methylene blue dye from brown macroalgaâĂŕ: effects of operating parameters, isotherm study and kinetic modeling. *J Clean Prod* **152**, 443–453.